Available online at www.sciencedirect.com
ScienceDirect
Polymer 49 (2008) 1635–1650
polymer
www.elsevier.com/locate/polymer

Molecular origins of toughening mechanism in uniaxially stretched nylon 6 films with clay nanoparticles

B. Yalcin [a], Z. Ergungor [a], Y. Konishi [a], M. Cakmak*, C. Batur [b]

[a] Polymer Engineering Department, University of Akron, Akron, OH 44325, United States
[b] Mechanical Engineering Department, University of Akron, Akron, OH 44325, United States

Received 15 December 2007; received in revised form 15 January 2008; accepted 17 January 2008
Available online 26 January 2008

Abstract

Introduction of nanoplatelets into the nylon matrix preorients the polymer chains in the film plane during melt casting leading to uniplanar (001) texture in nylon 6 crystalline as well as clay phase. This behavior enhances the uniformity of films during cold deformation well above the glass transition temperature by suppressing the localized necking behavior. The clay platelets reduce the polymer interchain hydrogen bonding and entanglements leading to decrease of long range ''connectivity''. As a result, a delay in strain hardening during deformation occurs allowing much larger deformations to be attained without fracture. This in turn leads to increase in toughness.

Keywords: Nylon 6 nanocomposites; Uniaxial stretching; Toughening

1. Introduction

The superior mechanical and barrier properties as well as a wide service temperature range make nylon 6 a prominent engineering thermoplastic. This semicrystalline polymer has numerous applications in automotive, electrical and packaging industries. Many of these applications profit from the high stiffness, toughness and tensile strength of nylon 6. Numerous methods have been developed to enhance its current properties and leading to its wider utility [1].

One conventional method for performance improvement involves inclusion of micron-sized fillers as reinforcing agents such as kaolin and fiberglass. The mechanical properties of the so-formed microcomposites are improved considerably relative to the bulk polymer when a tensile stress is generated in the filler through elongational and shear stresses applied through the matrix. However, such reinforcement requires the use of large filler concentrations (up to 40%) that leads to increased specific weight, brittleness and reduced optical clarity [2]. Recent studies on nylon nanocomposites [3–9] indicate a number of improvements in the performance of nylon 6 without the above-mentioned drawbacks of the traditional microcomposites. Natural layered silicates such as montmorillonite clay with the thickness in the nanometer range and the other two dimensions in the micron range provide reinforcement at much lower filler concentrations. With the addition of 2–10 wt% nanoplatelets, tensile and impact strength, and flexural modulus of nylon 6 are improved. The increase in room temperature tensile modulus of nylon 6 nanocomposite is as high as 168% [10].

There are many factors that establish the superiority of nanocomposites over microcomposites. In a layered-silicate polymer nanocomposites, where the silicate sheets are intercalated or exfoliated in the polymer matrix, the interfaces between the filler and the matrix constitute a much larger volume fraction of the bulk material. The amount of polymer affected by the abundant high surface area of the filler is thus larger in a nanocomposite and the increased coupling between the clay and polymer facilitates stress transfer to the reinforcement phase. The increased polymer–filler interaction has been proposed as a factor altering the toughening mechanism of nylon 6. Additionally, the nanosilicates contribute more to the

* Corresponding author.
E-mail address: cakmak@uakron.edu (M. Cakmak).

0032-3861/$ - see front matter © 2008 Elsevier Ltd. All rights reserved.
doi:10.1016/j.polymer.2008.01.046

modulus of a composite because the modulus is directly proportional to the aspect ratio of the filler. Thus, the high aspect ratio of the silicates, their unique intercalation and exfoliation characteristics and better adhesion at the polymer–clay interface determine the prominent property enhancement [11–15].

In melt processing, an important component of property enhancement is the orientation of clay platelets and polymer chains in the flow direction. Primarily, the nanoplatelets become substantially oriented in the flow direction and subsequently the polymer chains orient along with the clay sheets in processes such as injection molding [16,17] and fiber spinning [18,19]. Studies on the orientation of nanocomposites in shear flow also show that the clay platelets orient easily in the shear plane along which they show the lowest resistance to flow [20,21]. Although the studies on the orientation of clay sheets and polymer chains in melt flow are rather abundant [16,17,22–25] the research on the orientation behavior observed in uniaxial cold drawing of nanocomposite systems is rare [26].

This paper focuses on the effect of clay nanoparticles on the enhancement of mechanical extensibility and orientation behavior of melt-cast nylon 6 films during uniaxial stretching at temperatures between their glass transition, T_g, and melting temperature T_m. In order to assess the dynamical structural changes during deformation as influenced by temperature and composition, the true stress–true strain and birefringence were measured simultaneously to capture the evolution of structural and mechanical anisotropies and quantitatively investigate the mechano-optical properties. The system built and developed by our group allows us to measure the actual deformation levels in the sample locally and consequently the true stress–true strain behavior as well as the online birefringence of the deforming material. We have recently reported mechano-optical properties of a diverse range of polymers with distinct cases of crystallization behavior, i.e. fast crystallizing [22,27], slow crystallizing [28,29] and non-crystallizing [30,31], during uniaxial stretching. We have discovered that although each of these polymers exhibits complex and typically transient (linear to non-linear) mechano-optical behavior during stretching, the mechano-optical behavior can be generalized for polymers exhibiting similar crystallization behavior. We have shown that the deformation behavior and structural development during uniaxial stretching of polymers are very much influenced by their ability to crystallize (fast and slow crystallizing and non-crystallizing) and the physical state of the material (glassy, rubbery, partially molten and fully molten) which is determined by the temperature, speed and the extent of deformation employed in the stretching experiment.

In this paper, we present our mechano-optical studies and structural evolution analysis of nylon 6 nanocomposite films during uniaxial stretching at temperatures well above the glass transition ($T_g + 50$ °C, $T_g + 80$ °C and $T_g + 130$ °C) and focus on the origin of the expansion in solid state extensibility with nanoparticles.

2. Experimental methods

In this section, we describe the materials used in this study, instrumentation of the uniaxial stretcher, measured parameters and structural characterization techniques, i.e. wide angle X-ray diffraction (WAXD), small angle X-ray scattering (SAXS), transmission electron microscope (TEM) and attenuated total reflection (ATR).

2.1. Materials

Extrusion grade unfilled nylon 6 and nylon 6–montmorillonite nanocomposite pellets with 3 wt% and 5 wt% clay contents were received from RTP® Company. The nanocomposite formulation and compounding are confidential information and were not provided. However, we were assured that there were no ingredients other than nylon 6 and clay in the compounding formulation. This is important since plasticizers, additives or other impact modifiers used in compounding formulation could influence the structure and properties of nylon 6. Therefore, we can attribute all property changes in nylon 6 to the presence of Cloisite® 30B (Southern Clay) in the formulation. Cloisite® 30B from Southern Clay has been the most frequently used nanoclay grade for polymer nanocomposites. It is a natural montmorillonite modified with methyl, tallow, bis-2-hydroxyethyl, and quaternary ammonium. In this paper, we only studied nylon 6 nanocomposites with Cloisite® 30B. Clay modification influences the clay–polymer interaction. Hence, other clay grades with different organo-modifiers may influence the mechanical behavior of the polymer in a different way.

Prior to casting the as-received samples were dried for 24 h at 80 °C in vacuum oven. The films were then cast through Prodex 1 1/2-inch single screw extruder. The temperatures in zones 1–3 of the extruder were chosen as 240 °C, 250 °C and 275 °C, respectively, and the die temperature was set to 275 °C. The sheet was cast onto a 12 inch diameter chill roll maintained at 70 °C. The average thickness of the unfilled nylon and nanocomposite films was 150 μm and 80 μm, respectively. The films were kept in the freezer in airtight bags to reduce moisture uptake.

2.2. Instrumentation of the uniaxial stretcher and measured parameters

The uniaxial stretching experiments were carried out using a custom built instrumented uniaxial stretching system that allows the real time determination of true stress, true strain and birefringence simultaneously during deformation. Although the details of this equipment and measurements were given elsewhere [22,32,33], we revisit this section briefly.

Online spectral birefringence is essentially based on light intensity method [34]. In this method white light is used to get the order number of retardation automatically. Birefringence is measured by the ratio of the real time retardation values to the real time thickness values measured at the same time and at the same location. This is accomplished

using a laser micrometer mounted at an oblique angle that measures the width of the sample continuously. We then use the transverse isotropy (Eq. (1)) to calculate the real time thickness (Eq. (2)) with the knowledge of initial thickness. The true stress is defined as the ratio of the tensile force to the ''actual'' cross-section of the sample. In order to get the true stress (Eq. (4)), we directly measure tensile force by a load cell and divide it by the real time cross-sectional area of the film. The real time cross-sectional area of the film is the product of the width determined by the laser micrometer and the thickness (Eq. (2)). For elongation we define three parameters, i.e. stretch ratio, engineering strain and true strain. Stretch ratio is the ratio of the final length of the stretched sample to its initial length. Engineering strain is defined as the ratio of elongation (difference between the final length and the initial length) to the initial length of the sample. As for the true strain, we relate the state of elongation directly to the reduction in the local width of the sample. This is the same local region (mid-region of the sample) where the retardation measurements are made. We then combine the transverse isotropy (Eq. (2)) with the incompressibility assumption (Eq. (3)) and determine the true strain (Eq. (5)).

$$W_t/W_0 = D_t/D_0 \tag{1}$$

$$D_t = (W/W_0)D_0 \tag{2}$$

$$D_0W_0L_0 = D_tW_tL_t \tag{3}$$

$$\text{True stress} = \text{force}/\text{cross-sectional area} = F_t/W_tD_t = F_t/\left[\left(W_t^2/W_0\right)D_0\right] \tag{4}$$

$$\text{True strain} = \text{elongation}/\text{initial length} = (L_t - L_0)L_0 = \Delta L/L_0 = (W_0/W_t)^2 - 1 \tag{5}$$

where W_t is real time width of the film, W_0 is initial width of the film, D_0 is initial film thickness, D_t is real time film thickness, L_0 is initial length of the film, L_t is real time length of the film, and F_t is force.

2.3. Stretching and material parameters

Dumbbell shaped samples with 30 mm gauge length and 25 mm width were cut from the as-cast sheets for all the stretching experiments. A constant crosshead speed of 50 mm/min was employed for each experiment.

Samples were stretched at 100 °C, 140 °C and 180 °C to a total engineering stretch ratio of 4. These temperatures are well above the glass transition temperature and well below the peak melting temperature (T_m) of nylon 6 and its nanocomposites as shown in Fig. 1. The clay content in nylon 6 was 0 wt%, 3 wt% and 5 wt%.

The relaxation behavior was monitored for 30 min, while the samples were constrained at the final stretched state at the drawing temperature. To investigate the effect of deformation on properties, the latter experiments were performed for samples that were stretched to a range of stretch ratios from 1.5 to 4.

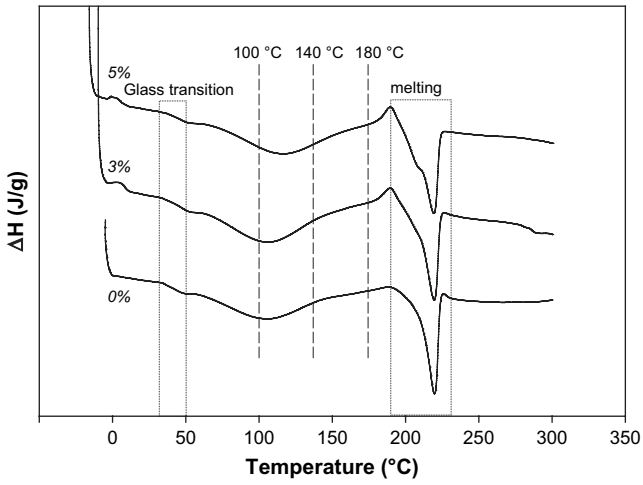

Fig. 1. DSC of unfilled nylon 6 and its nanocomposites with montmorillonite clay.

2.4. Structural characterization

2.4.1. Wide angle X-ray diffraction (WAXD) and small angle X-ray scattering (SAXS)

The effects of nanoparticles, stretching temperature and deformation on the developed crystalline structure in uniaxially stretched films were analyzed both by WAXD and SAXS. WAXD was performed on a BRUKER system operated at 40 kV and 40 mA. SAXS patterns were obtained using S-Max3000 Rigaku SAXS system. The samples were exposed to X-ray in their as-cast (unstretched) and stretched forms with the beam directed both along the thickness (normal) and the width (transverse) direction to assess the superstructural order and orientation in crystalline phase of the polymer as well as clay particles.

2.4.2. Small angle light scattering (SALS)

Small angle light scattering was performed in order to identify the initial superstructure present in the as-cast unfilled nylon 6 films. A 2 mW 632.8 nm He–Ne with beam size of 1 mm was used as the source of polarized monochromatic light. Hv pattern was obtained with the polarizer and analyzer oriented in TD and MD of the films, respectively. The patterns were captured using a 16-bit CCD camera software (Photometrics-cooled CCD) operated by IPLab spectrum.

2.4.3. Attenuated total reflection (ATR) study

ATR analyses were carried out on unstretched and stretched samples at different true strain levels in order to determine the crystal phase transformation and state of hydrogen bonding. ATR analyses were performed using EXCALIBUR Series DIGILAB FTS 3000. The spectra were normalized using the carbonyl stretching vibration band at 1630 cm^{-1}.

2.4.4. Transmission electron microscopy (TEM)

All TEM images were taken at room temperature by a Philips TEM (Model FEI-TECNAI 12®) operated at 120 kV. The images were recorded under scanning Gaussian focus with bright-field image mode. In order to investigate the orientation of clay nanoparticles in unstretched and stretched samples, ultrathin (25–50 nm) samples were sectioned from the surface (MD–TD) and side plane (MD–ND) of the films. MD, TD and ND denote machine (length), transverse (width) and normal (thickness) directions, respectively. The sampling planes are indicated on each TEM image.

3. Results and discussion

3.1. Structure of as-cast films

The clay particles, having very high aspect ratios, tend to orient easily when the melt containing them is subjected to flow fields. Therefore, it is nearly impossible to obtain melt-cast films that are completely isotropic. This was shown for the first time by Toyota researchers in early 1990s for melt-cast films of nylon 6 nanocomposites [35]. The clay platelets and the crystallites were aligned parallel to the film surface in the machine direction. Bafna, Beaucage and their coworkers reported similar structures in thin (50 μm-end thickness) melt-cast films of high density polyethylene (HDPE) reinforced with organically modified clay using 2D SAXS and WAXD [36]. Their detailed 3D orientation study showed that the clays were oriented parallel to the film surface with their normal perpendicular to the machine and transverse directions. Galgali et al. reported anisotropic structure for much thicker (1000 μm-end thickness) melt extruded syndiotactic films of polypropylene using 2D WAXD [37]. Anisotropic orientation structure was even shown for solution cast PEO nanoclay films prepared by blade spreading method [38]. In the light of these earlier studies, we decided to quantify the initial structure present following melt casting. For this, we utilize WAXD, SAXS, SALS and TEM techniques. Initial structure evaluation is important for subsequent uniaxial stretching analysis.

Unfilled nylon 6 films exhibit Hv SALS four-leaf-clover pattern with maximum intensity along the radial direction at 45°-azimuthal evidencing the presence of spherulitic structure. This is shown in Fig. 2. The SALS pattern does not change when the sample is rotated between the cross polarizers indicating that the sample is isotropic in the plane. WAXS patterns also confirm that the crystalline regions are randomly oriented. These results are not unexpected as nylon 6 is a fairly fast crystallizing polymer exhibiting low shear viscosity due to its naturally low molecular weight that are not readily oriented and if oriented, the chains rapidly relax into isotropic form upon casting on a chill roll.

The addition of 3 wt% clay particles to the melt-cast nylon 6 films results in the appearance of anisotropy that depends on the direction of X-rays relative to ND and TD as illustrated in Fig. 3a and b. The film exhibits nearly isotropic WAXD pattern when X-rays are directed in the ND (Fig. 3a) with slight preferential orientation (Fig. 4b) in the machine direction

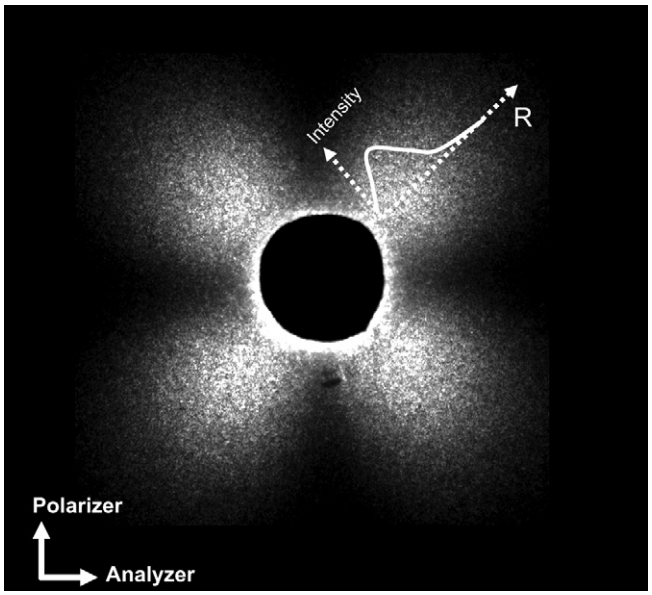

Fig. 2. Small angle laser light scattering four-leaf-clover pattern of melt-cast unfilled nylon 6 samples. This pattern does not change when the sample is rotated in the plane between crossed polarizers.

indicating the presence of nearly in-plane isotropy. The same sample exhibits a very high anisotropy when the WAXS pattern is obtained with X-rays directed along the TD (Fig. 3b). In this pattern, high preferential orientation of (020) planes along the extrusion direction (MD) is observed. The polymer chains are highly oriented in the MD–TD plane of the films as the (020) plane poles are parallel to the chain axes in nylon 6 crystals, which exhibit mostly monoclinic crystal form both in the alpha (α) [39] and gamma (γ) [40] phase. In addition to the chain axis, *a*-axes of the unit cells are also oriented in the film plane while the *c*-axes are oriented normal to the film plane as evidenced by the orientation of (001) planes. The increase of clay concentration to 5% does not significantly change the latter behavior, as it is evident in the WAXD patterns. From these observations we can conclude that the addition of clay promotes nearly uniplanar (001) texture in nylon 6 crystalline phase.

This is further evidenced in Fig. 5 showing the increase in azimuthal spread of (020) planes as the nanocomposite film sample is rotated about the MD. In Fig. 5, *b**-(020) reflection was image enhanced for ease of observation. In this figure, at zero degrees of rotation, i.e. $\omega = 0$, one can also notice an oriented streak pattern at small angles close to the beam stop. This pattern is from the clay platelets and evidences preferential orientation of the platelet surfaces parallel to the film surface (in MD–TD plane) as well. As a result of the latter preferential orientation of the platelets, when the sample is rotated 45° about the MD, the streak pattern disappears. This preferential orientation of the platelets with their broad surfaces parallel to the MD–TD plane is also confirmed with the TEM image taken on the MD–ND plane (thickness plane) in Fig. 6. Edges of the well-dispersed platelets appear as dark lines as the electrons passing through the clay particles oriented edge-on shows the highest absorption. As it is apparent

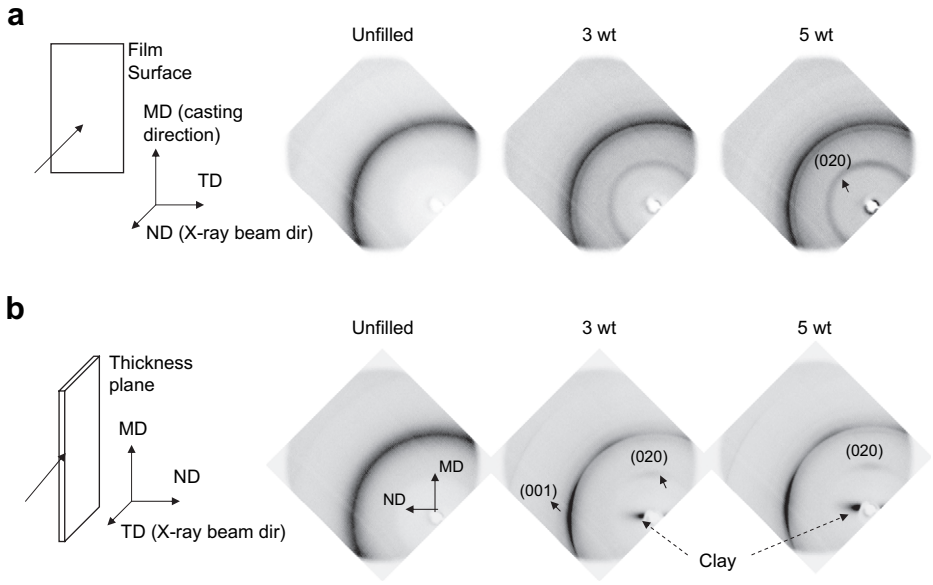

Fig. 3. WAXD patterns of as-cast unfilled nylon 6 and nylon 6/clay nanocomposites. (a) MD–TD plane and (b) MD–ND plane.

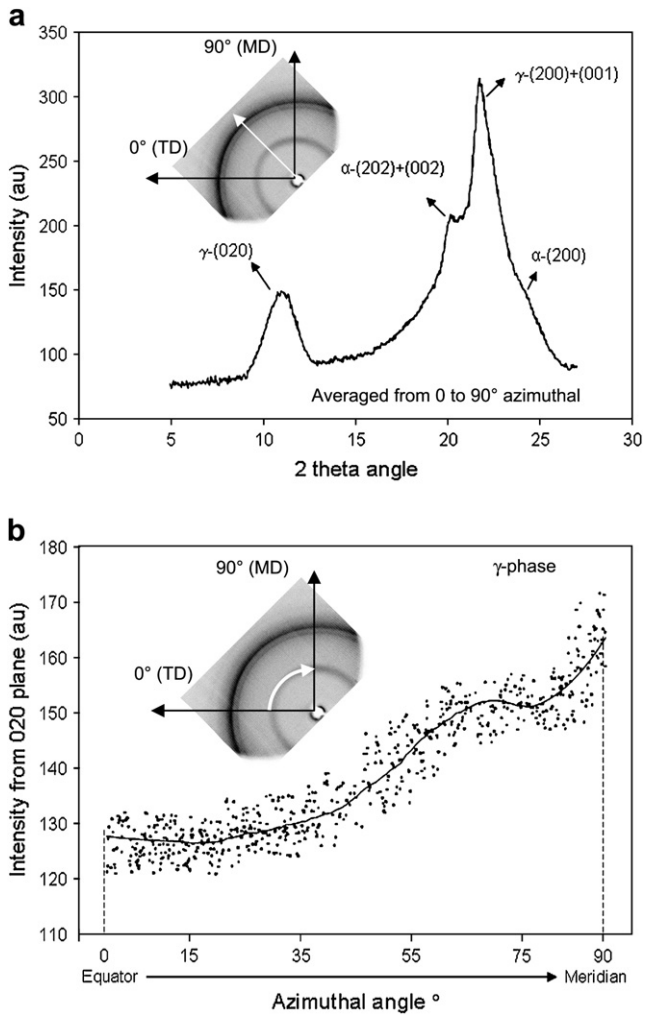

Fig. 4. (a) WAXD 2θ scan and (b) WAXD patterns of 5% nanocomposites showing slight anisotropy along the azimuthal direction (X-ray direction: ND) (020) planes.

in Fig. 6 and the TEM images in subsequent figures, the clay is well dispersed in nylon 6 with substantial exfoliation and a small amount of stacked clay agglomeration.

SAXS technique also reveals by large planar orientation behavior of the clay to the film surface as shown in Fig. 7. With these patterns, we also assess the superstructural organization in nylon 6 phase as well. When the X-ray beam is directed along the ND, the unfilled sample shows an isotropic SAXS discrete ring. This is roughly the same in the 3% and 5% clay filled films with SAXS patterns taken with X-ray beam directed along ND. The long period pattern shows slight orientation along the original extrusion direction. When the X-rays are directed along TD, the 3% clay filled film exhibits two distinct patterns. One is the very strong equatorial streak that is due to near parallelism of the clay particles oriented in the MD–TD plane in real space. Since there is a fair amount of distribution of separation distance between the platelets, this translates to the broadening of the streak in the normal direction. The equatorial streak is very strong due to the very large difference between the density of montmorillonite, ~2.7 g/cm^3 and the nylon 6 phase (crystal density = 1.23 g/cm^3, amorphous density = 1.09–1.10 g/cm^3). Additionally, some degree of azimuthal spread of the streak patterns indicating that the parallelism of the platelets in the MD–TD plane is not perfect is also evident in TEM photomicrograph shown in Fig. 6. In addition to the high intensity streak scattering pattern, one can also observe lower intensity meridional discrete scattering as a result of spatially periodic density fluctuations due to alternating crystal–amorphous phases. Unfilled nylon 6 displays no orientation regardless of the SAXS beam direction, similar to what we have seen in WAXD. Nanocomposite samples, on the other hand, display a discrete two point pattern particularly when the X-ray beam is in the TD. When the X-ray beam is along the ND, however, the two point pattern spreads significantly in the azimuthal direction displaying

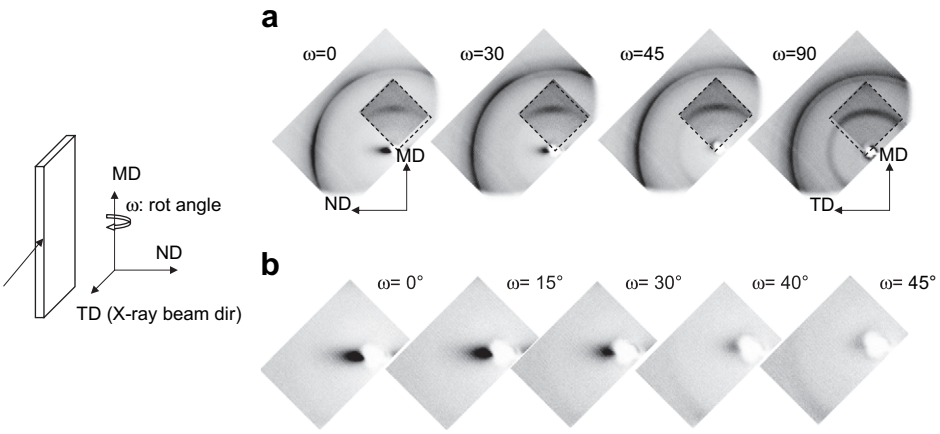

Fig. 5. WAXS patterns of 3 wt% nylon 6/clay nanocomposites. X-ray beam is in TD. The sample is rotated about the MD axis from 0° to 45°.

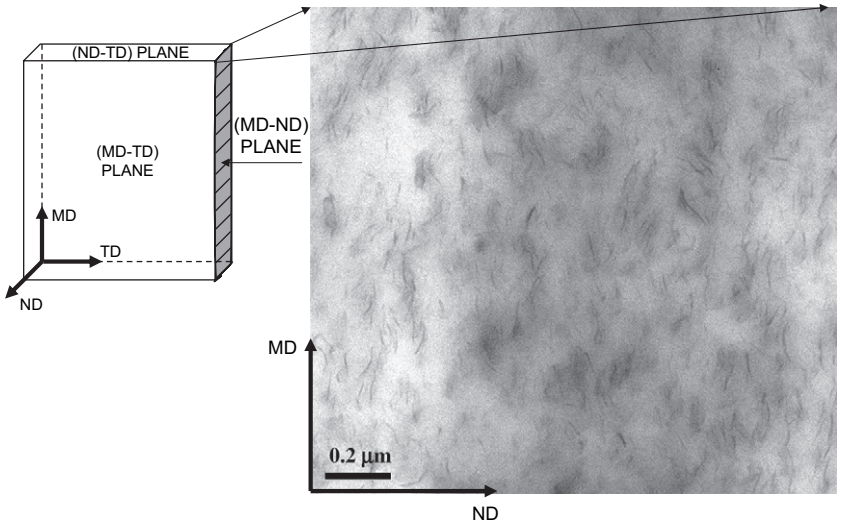

Fig. 6. TEM image of as-cast 3 wt% nanocomposite film in the MD–ND plane (thickness plane). Shaded area is the plane where TEM is taken.

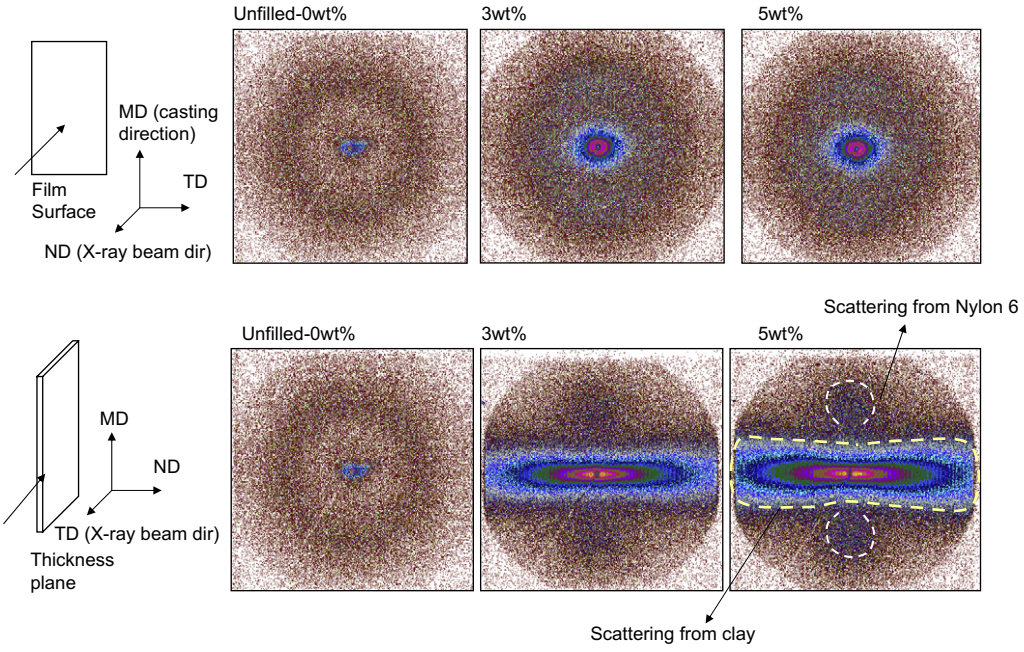

Fig. 7. SAXS patterns of as-cast films.

almost a continuous ring. This direction dependent pattern formation is the same behavior we have seen in WAXD. SAXS patterns also confirm that there is nearly planar orientation of the lamella in the film plane (MD–TD). The lamellae with the folded chain axes rotate in the MD–TD and to some extent about the MD axis but lack the third rotational freedom about the TD.

Fig. 8 summarizes the overall texture exhibited by the presence of clay nanoparticles in the cast films. As the data so far clearly illustrate, the clay particles become oriented well inside the die while they are subjected to extensional/shear through converging flow before exiting the die lips. This clay orientation also promotes the crystallization behavior of nylon 6 by acting as nucleation surfaces. In these samples, the preferred crystal growth direction is the *c*-axis while the *a*–*b* planes orient parallel to the clay particles. We also observe some degree of preferential orientation in the extrusion direction even though no significant take up was applied to the films during their solidification. The observed orientation in the as-cast nanocomposite films could also be generated by the shear amplification effect in the chains caught between the adjacent nanoplatelets during the flow in the die. Because of the decrease in orientation relaxation due to the rigidifying effect in the chains in the vicinity of the clay particles, the developed orientation can remain in the films even after the solidification takes place. We conclude that the overall texture is formed mostly by the epitaxial growth of the polymer crystals on the clay platelets with the primary crystal growth direction along the *c*-axis that becomes normal to the film plane and partially by the shear amplification combined by significant decrease in orientation relaxation. In our earlier studies with high shear injection molding process of nylon 6, we have shown shear amplification mechanism to be much more effective than this melt-casting process where the melt is subjected to relatively gentler shear history [16,17].

As for the crystal phase in the as-cast samples, both unfilled nylon 6 and nanocomposites display mainly γ-form. There is a trace amount of α-form of nylon 6 in the 5 wt% nanocomposite. The influence of stretching on the development of crystal phase will be discussed below.

3.2. Mechanical and structural behaviors of unfilled nylon 6 and nanocomposites during uniaxial stretching

In this section, we will investigate the structural and mechanical behaviors of nylon 6 films during stretching as influenced by the nanoparticles and stretching temperature. We will first examine unfilled nylon 6 at the lowest stretching temperature, 100 °C. Fig. 9 shows the stretching behavior of unfilled nylon 6 with four different curves, i.e. engineering stress–engineering strain (Fig. 9a), true stress–true strain (Fig. 9b), birefringence–true stress (Fig. 9c) and birefringence–true strain (Fig. 9d). Three distinct points are marked on these curves as I, II and III corresponding to the important phenomena taking place during stretching.

First point (I) is the yield point which occurs beyond a true stress value of 24 MPa and is best recognized in the engineering stress–engineering strain data (Fig. 9a). Yield point is less obvious in the true stress–strain data (Fig. 9b) because the true stress calculation uses the actual value of the decreasing cross-sectional area of the sample during stretching and hence is less sensitive to the necking associated local reduction in the width of the sample. In the birefringence–true stress curve (Fig. 9c), the yield point corresponds to the deflection point beyond the initial birefringence plateau and is characterized

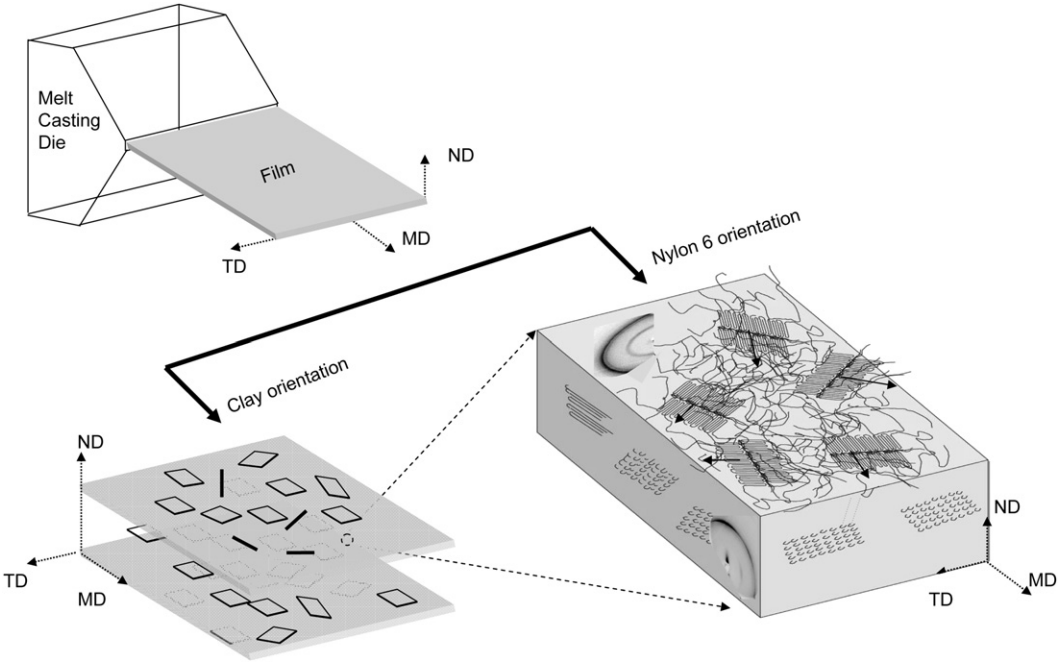

Fig. 8. Model for nylon 6 and clay orientation in as-cast nanocomposite films.

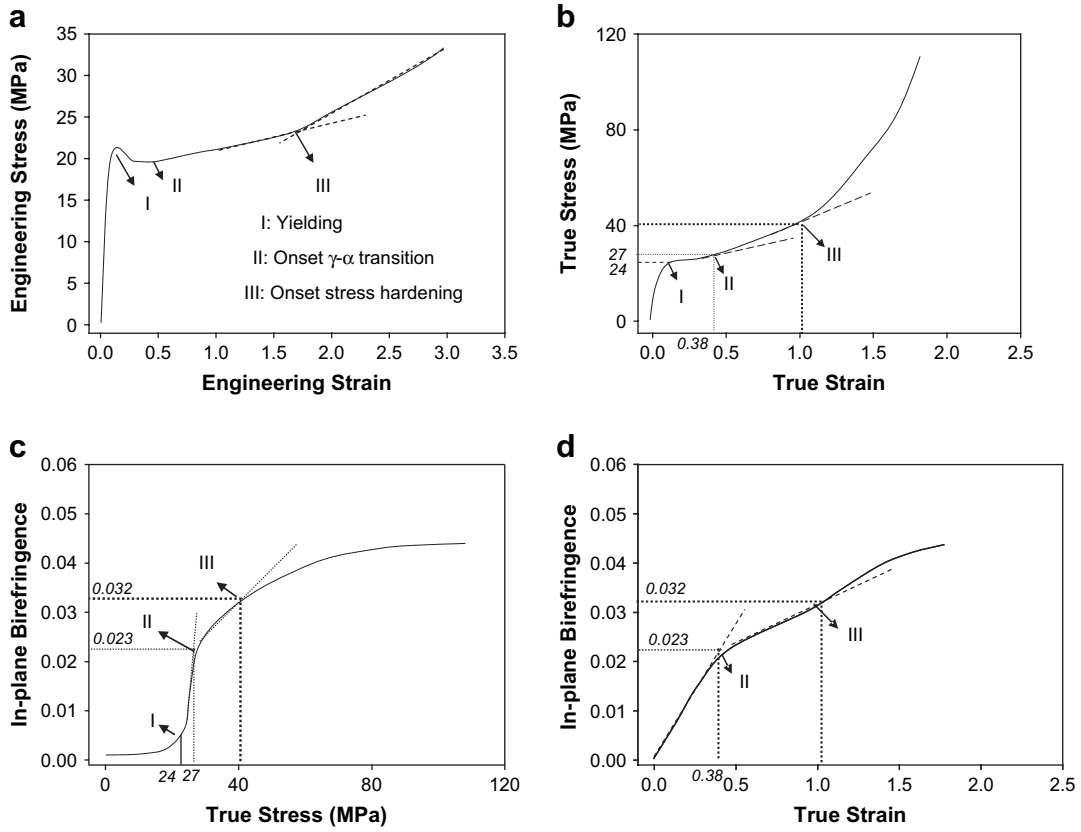

Fig. 9. Nylon 6 films at 100 °C. (a) Engineering stress–engineering strain, (b) true stress–true strain, (c) birefringence–true stress, and (d) birefringence–true strain.

with a steep rise of birefringence when the true stress value reaches 24 MPa.

The second point (II) is associated with the strain induced crystal transition of nylon 6 from gamma (γ) to alpha (α) phase [41–43]. The crystal transition is best recognized in the birefringence–true strain curve (Fig. 9d) by a negative deviation from the initial linear regime at a true strain value of 0.38 and a birefringence value of 0.023. The negative deviation, i.e. decrease in the rate of birefringence increases with true strain, is due to the fact that the newly formed (α) alpha crystals are less ductile and deformable than the original gamma (γ) crystals [44–46]. This results in smaller increase in birefringence during stretching. This occurs in spite of the higher intrinsic birefringence (0.097) [47], (0.094) [48] values reported for (α) alpha crystals than gamma (γ) crystals (0.066 [48]). Ito et al. proposed that the plastic deformation in nylon 6 involves chain slip with hydrogen bond rupture and that the superior ductility of gamma (γ) crystals over the alpha (α) crystals was due to the lower hydrogen bond density in gamma (γ) crystals. Lin et al. reported that the plasticity in nylon 6 was governed by the crystal slip parallel to the H-bonded sheets without breaking of the H-bonds and the intersheet distance between the H-bonded sheets, i.e. (200) spacing, was larger for the gamma (γ) crystals than the alpha form and required lower shear stress levels for deformation to take place [45]. The onset of crystal transition, i.e. the second point (II), is also apparent in the birefringence–true stress curve in Fig. 9c. It manifests itself by a negative deviation of the birefringence following its steep rise after the yield point. True stress–true strain data, though less obvious, also evidence the crystal transition point by a positive deviation during plastic deformation following the yielding point. Since the alpha (α) crystals are less ductile and have lower H-bonded intersheet distances, they require more stress for crystal slip deformation and hence a positive deviation takes place. Our real time mechano-optical measurement system proves to be a convenient tool to monitor the rapid (γ)–(α) crystal transition during stretching. The crystal transitions identified on the mechano-optical curves (Fig. 9b–d) is supported in Fig. 10 by the ATR and WAXD scans. One can clearly see that the peaks associated with alpha crystal phase develop at a true strain value of 0.38. The initial gamma (γ) crystal structure in unfilled nylon 6 changes to alpha (α) form around 1.4× stretch ratio which corresponds to 0.38 true strain value as observed in the birefringence–true strain data (Fig. 9d).

The third point (III) is associated with the onset of stress hardening where the crystals approach their limit of extensibility. This point is most obvious in true stress–true strain (Fig. 9b) and birefringence–true stress (Fig. 9c) curves and manifests itself by a rapid rise of stress while the rate of increase in birefringence and true strain approaches zero.

In summary, stretching at 100 °C initially sets off a sharp increase until the yield point where the slip of the gamma (γ) crystal planes parallel to the H-bonded sheets occurs at

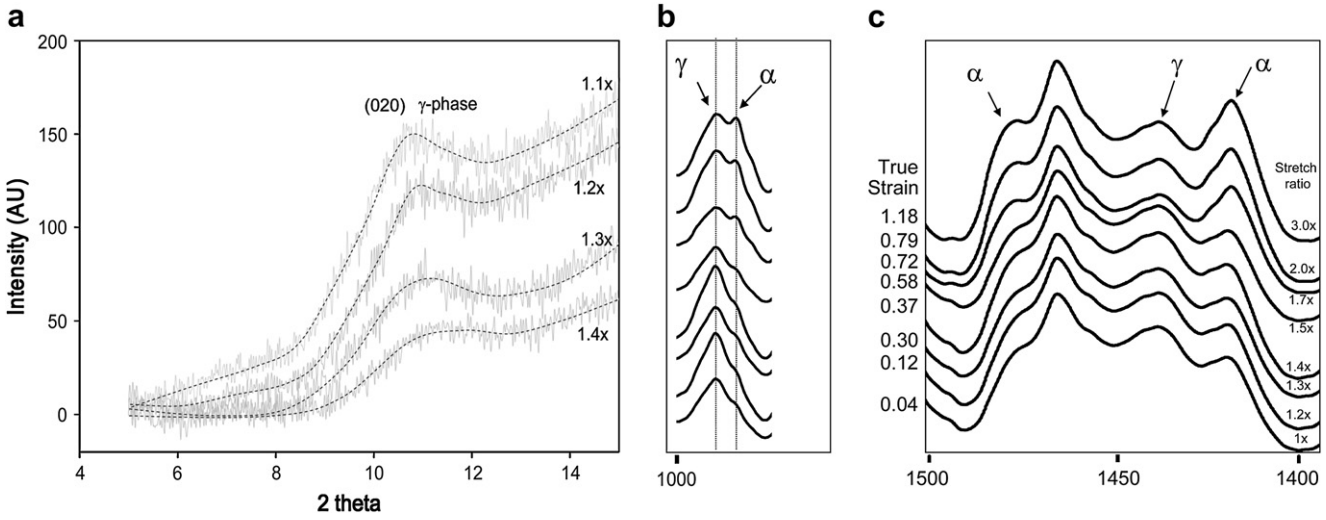

Fig. 10. γ to α crystal transition with stretching. (a) 2θ WAXD, (b and c) ATR.

a critical stress value of 24 MPa. The initial spherulitic structure of unfilled nylon 6 goes through the yield point with a stress drop and continues to deform with a crystal transition into alpha (α) form at about 38% true strain. Eventually the crystals approach their maximum limit of extensibility at 100% true strain and start to exhibit strain hardening. We will examine the crystal structure during stretching in the upcoming sections.

3.2.1. Nanoparticle effects

Having established the general pattern for unfilled nylon 6, we now examine the same curves with the three points of interest (I–III) as influenced by the nanoparticles and temperature. In our investigations, we will focus on the curves that best describe and clearly distinguish each phenomenon. For instance, for the investigation of the crystal transition, we will examine the birefringence–true strain curves.

The initial stages of the engineering and true ''stress–strain'' curves of unfilled nylon 6 films at 100 °C, 140 °C and 180 °C and the nanocomposites at 100 °C are presented in Fig. 11. The stretching temperature and the presence of the nanoplatelets have a marked influence on the yield behavior and hence the necking of nylon 6. Increasing the stretching temperature reduces the yield stress as well as the stress drop beyond the yield stress. The presence of nanoplatelets increases the yield stress but decreases the stress drop beyond the yield stress and hence alleviates the necking in the films. Since the nanocomposites already contain oriented small crystallites and nanoplatelets in the cast film, the material properties are more uniform and the localized reduction of the yield stress due to fluctuation in material properties, i.e. chain orientation, crystallinity, etc., in a given element is reduced. One can also see that the initial slope is higher in the nanocomposite implying increasing modulus, thus stiffness of the system as has been observed by others [10]. Increased modulus and yield strength confirm that nanoparticles act as reinforcing inclusions. The increase in modulus is also partially due to the presence of preferential orientation in as-cast nanocomposite films.

In Fig. 12, we display birefringence–true strain and birefringence–true stress curves of nylon 6 at three different nanoparticle loading levels, i.e. 0 wt%, 3 wt% and 5 wt% and stretching temperatures, i.e. 100 °C, 140 °C and 180 °C. The small vertical arrows on these curves indicate the points where the first negative deviation, i.e. gamma (γ) to alpha (α) transition, occurs as we have established earlier. One can notice that there is a critical birefringence zone at around 0.02 above which the crystal transition occurs. This zone is indicated by a striped rectangle on the curves. This is valid regardless of the nanoparticle loading and stretching temperature. This implies that once the nylon 6 molecules reach a critical level of birefringence, the transition begins to occur. Obviously, this critical level of birefringence is not reached at the same true strain and true stress when different nanoparticle loading or the stretching temperature is employed. In fact, there is a slight delay in true strain when the nanoparticle loading and stretching temperature are increased. However, one can conclude that orientation birefringence determines the onset of crystal transition. It was proposed by Miyasaka and Makishima [42] that for gamma (γ) to alpha (α) transition to occur, two conditions must be satisfied. First, there must be sufficient extension for the (γ) phase to untwist the chain around the amide group. Second, there has to be sufficient translational mobility of the chain to change the stacking in the crystallite.

Fig. 13 compares the entire ''engineering'' and ''true'' stress–strain profiles of ''unfilled'' nylon 6 stretched at 100 °C, 140 °C and 180 °C. Following the elastic and yield regions, stress increases gradually until the strain-hardening region. The ''apparent'' onset of strain hardening, i.e. third point (III), is noted by arrows in each curve. In the engineering stress–strain curves, the onset of strain hardening decreases with increasing temperature. In the true stress–strain curve, on the other hand, the onset of strain hardening shows almost no dependency with stretching temperature. There appears to be a critical true strain level above which the strain hardening

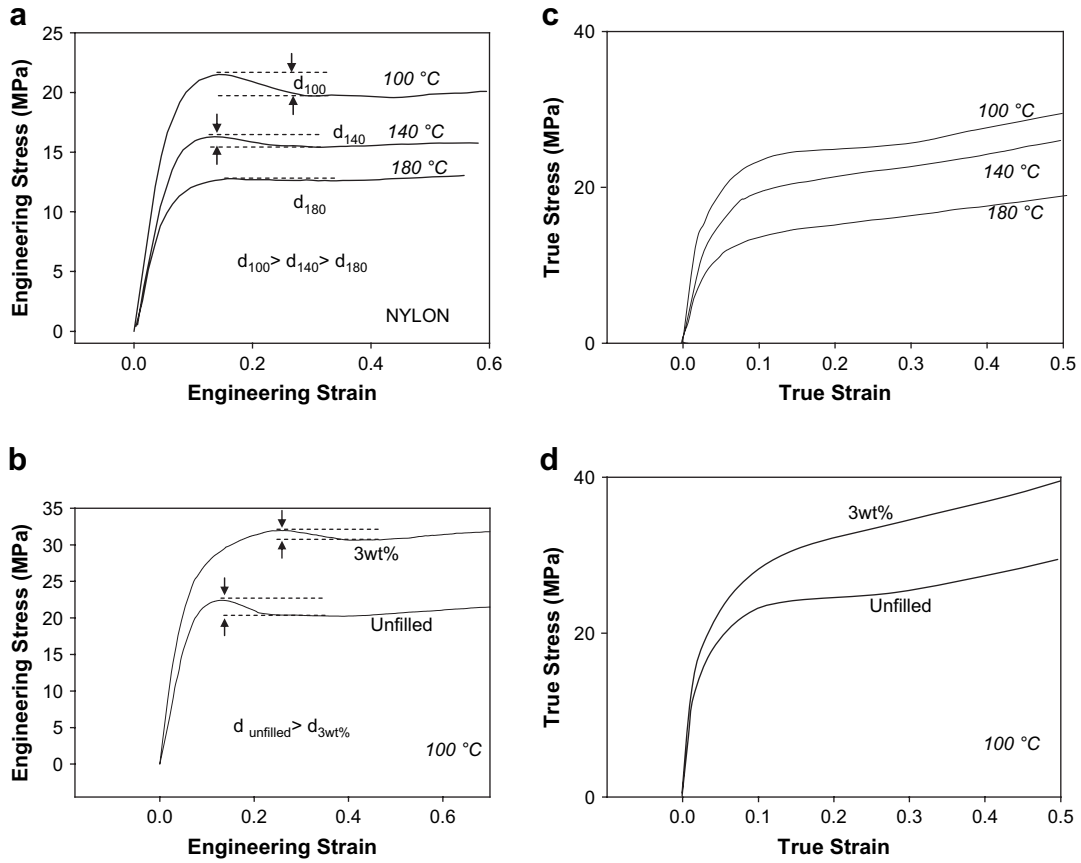

Fig. 11. Small strain initial yielding behavior. (a) Engineering stress vs. engineering strain (unfilled nylon 6 temperature effect). (b) Engineering stress vs. engineering strain (composition effect). (c) True stress vs. true strain (unfilled nylon 6 temperature effect). (d) True stress vs. true strain (composition effect).

takes place. This is due to the absence of orientation relaxation at these ''cold'' drawing temperatures. Although the onset of strain hardening is nearly the same for all temperatures, one can see that the development of strain hardening becomes more pronounced at lower temperatures. At higher temperatures such as 180 °C, strain hardening develops rather gradually. One can also notice that the stress levels in the engineering data, especially towards the final stages of stretching, are highly underestimated since the reduction of the cross-section during stretching is not taken into account for stress calculation.

In Fig. 14, the true stress–true strain and birefringence–true stress behaviors of unfilled nylon 6 are compared to those of nylon 6 nanocomposites with 3% and 5% clay loading. All these samples were stretched to the macroscopic draw ratio of 4 at 100 °C. In the plastic deformation and strain-hardening regions, stress levels of the 5% nanocomposite films are always larger than those of the 3% nanocomposites. The true stress values of the unfilled nylon films are the lowest at strains levels below ~1.4. However, unfilled nylon 6 reaches the strain-hardening point at a lower strain than the nanocomposites and displays a sharper increase in this region crossing over the two curves belonging to the 3% and 5% nanocomposites. Similar behavior is seen in the birefringence–true stress curve where unfilled nylon 6 exhibits higher birefringence level initially but reaches its limit of orientation more rapidly exhibiting a plateau region whereas the nanocomposites continue to deform more gradually and eventually attain higher birefringence levels than the unfilled nylon 6. This change in mechanism of strain hardening and enhanced extensibility of nanocomposite films is due to multiple factors. The first factor is the disruption of the hydrogen bonded nylon 6 network structure by the clay nanoplatelets. High strength levels acquired in nylons are almost certainly due to the presence of hydrogen bonds between the amide groups. However, these interchain bonds are considered to be an impediment to ultra-drawing of high molecular weight polyamides [49]. There have been studies in the literature attempting to reduce the cohesion energy E_c between polyamide chains through the suppression of hydrogen bonding via complex formation with strong Lewis acids [49,50]. Tonelli and Kotek [49] also suggested that mixing with nylon inclusion compounds may provide a way to eliminate hydrogen bonding during drawing, thus allow enhanced orientation. In a similar manner the nanoplatelets in nylon 6 act as separators to the chains and disrupt the hydrogen bonding rendering a looser network with less number connectivity between them as they also reduce the number of interchain entanglements. This suppresses the rapid rise of stresses associated with the strain-hardening process. At the strain levels close to the crossover strain, the unfilled nylon breaks but the nanocomposites are able to stretch further and eventually reach larger strain and stress levels before

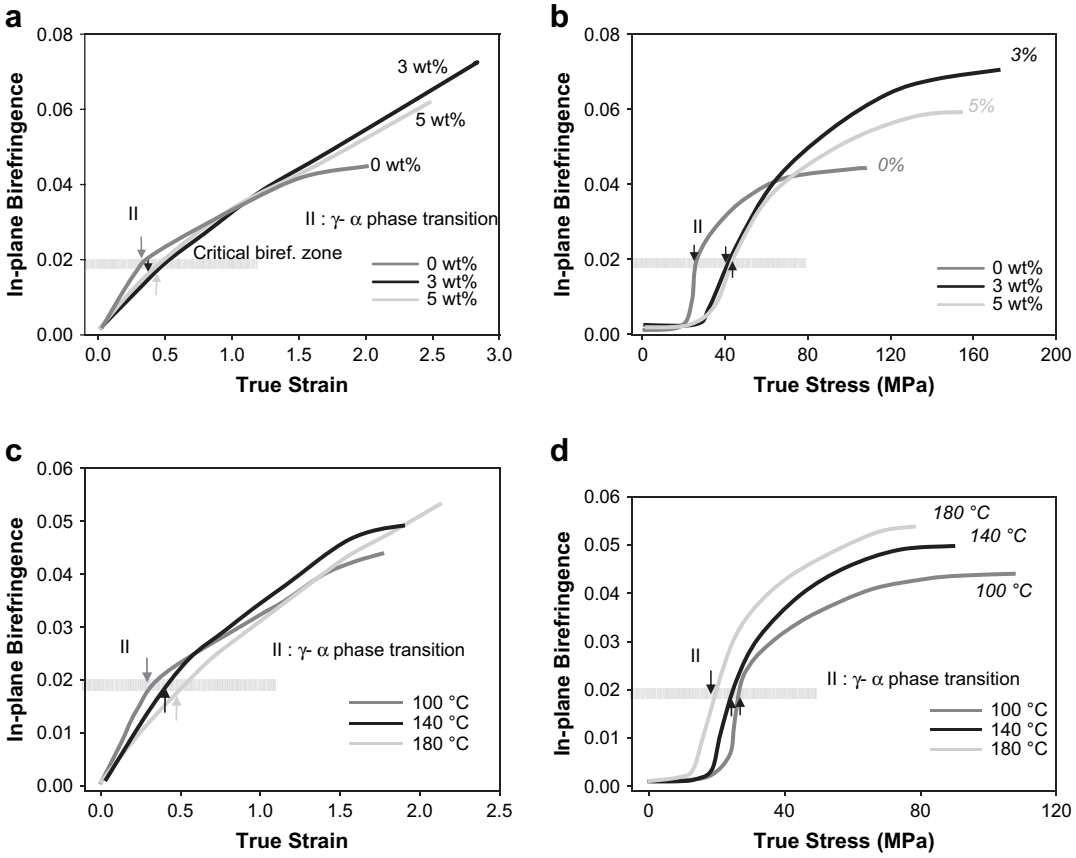

Fig. 12. Birefringence–true strain and birefringence–true stress behaviors as a function of (a and b) clay loading (0%, 3%, 5% clay) and (c and d) stretching temperature.

breaking (Fig. 14a). This enhancement of ultimate strain and stress levels displayed by the nanocomposites validates enhanced toughness brought about by partial dissociation of the nylon 6 network by the nanoplatelets. The disruption of hydrogen bonding in the nanocomposite systems is evidenced in Fig. 15 by comparing the absorbance levels of N–H stretching in the normalized ATR spectrum of the samples between 3200 cm^{-1} and 3400 cm^{-1}. At this point, it is important to note that we do not rule out the possible hydrogen bonding between the clay surface, the modifier and the nylon 6 chains. However, the number of hydrogen bonding cohesion points formed between the clay and the polymer does not compensate the ones hindered due to the presence of clay between the nylon 6 chains. Along with the partial dissociation of the hydrogen bonding, the second complementary factor that contributes to the increased toughening and extensibility in the nylon 6 nanocomposites is the ability of the nanoparticles to move and orient easily even under low shear deformation fields. This is due to the geometry of their surfaces with high aspect ratios and thicknesses in the nanometer range. Otherwise, one could think of other micron-sized fillers that have the potential of eliminating hydrogen bonding. However,

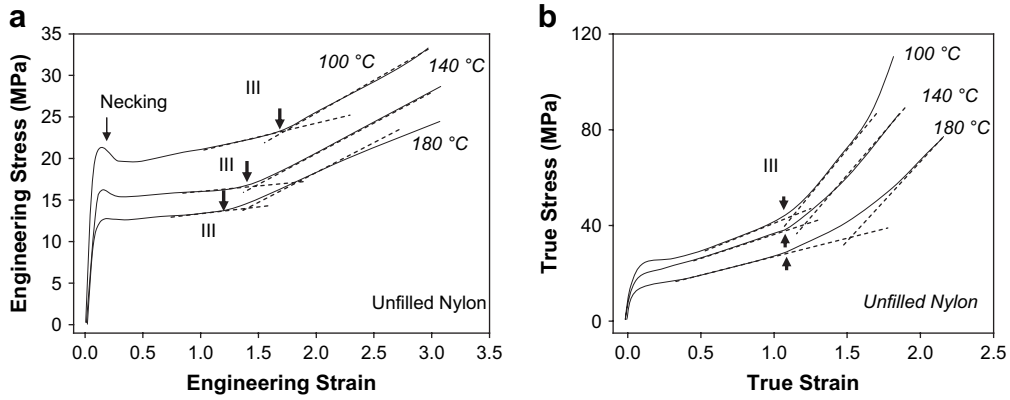

Fig. 13. (a) Engineering stress vs. engineering strain of nylon 6 at 100 °C, 140 °C and 180 °C. (b) True stress vs. true strain of nylon 6 at 100 °C, 140 °C, 180 °C.

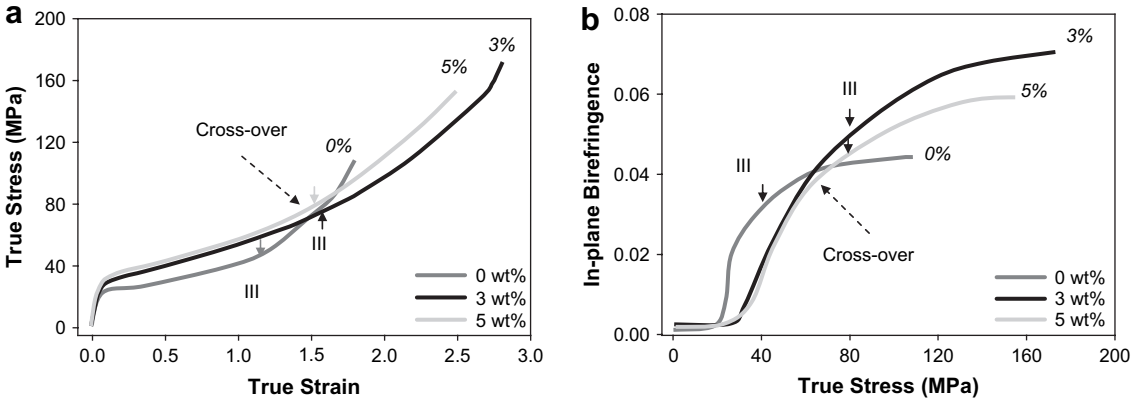

@100°C	Modulus (MPa)	True Strain %
unfilled	3.9	175
3wt%	5.4	277
5wt%	6.6	250

Fig. 14. True stress–true strain and (b) birefringence–true stress behaviors of 0%, 3%, 5% nanoclay filled nylon 6 films at 100 °C (arrows indicate strain hardening point).

such larger fillers promote brittleness. This is because those micron-sized fillers do not move or orient as readily as the nanoplatelets. Yet, another factor is the slippage of the easy shear planes, i.e. the (001) planes of polyamide 6 containing the H-bonds, which have an initial preferred orientation around the platelets as we have seen from WAXD patterns. The flow stress is lowered in thin interparticle matrix ligaments separating the nanoplatelets allowing the matrix to deform to large strains. In the strain-hardening region, it becomes increasingly difficult to deform the chains further because increasingly less number of slip systems remains favorably oriented to assist the deformation. Other studies showed that smaller particles and increased polymer–filler interaction promote toughening [51–53]. However, in this case we believe that nylon 6 has sufficient and perhaps too much of a network association for exhibiting reasonable toughness. Using the nanoplatelets one can optimize the amount of network associations for increased toughening. In fact, when the clay content is increased to 5%, there is too much of a network dissociation which adversely affects the extensibility of the films. The films become stiffer and less connected resulting in declined stretching behavior, while still exhibiting substantially improved behavior over unfilled nylon 6.

In summary, nylon 6 filled with small amounts of clay nanoplatelets promotes significant toughening because (1) certain number of interchain hydrogen bonding is eliminated, loosening the strongly connected network that causes early strain hardening. (2) Unlike stiff micron-sized fillers, the platelets orient and conform easily to the energetically favorable positions within the deforming network [16]. (3) The nanoplatelets are not entirely free from interactions from nylon 6 and there is a slippage of easy shear planes of preferentially oriented small nylon 6 crystallites in the as-cast films, i.e. (001). (4) The presence of large nanoplatelets also decreases the interchain entanglements.

3.2.2. *Influence of stretching on the clay (montmorillonite) orientation and crystalline structure*

Fig. 16 compares the TEM and SAXS images of an as-cast nanocomposite sample (3 wt%) with its stretched counterpart. The images were taken on the thickness plane (MD–ND). It is clear that uniaxial stretching promotes orientation in the

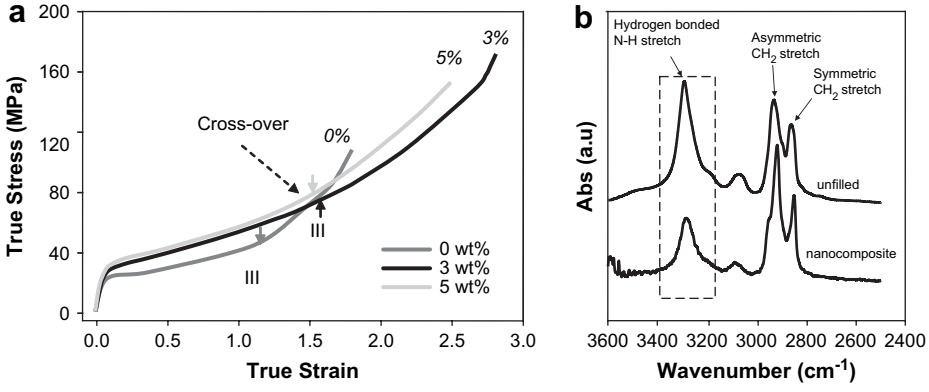

Fig. 15. Normalized ATR spectrum of unfilled nylon 6 and nylon 6 nanocomposites.

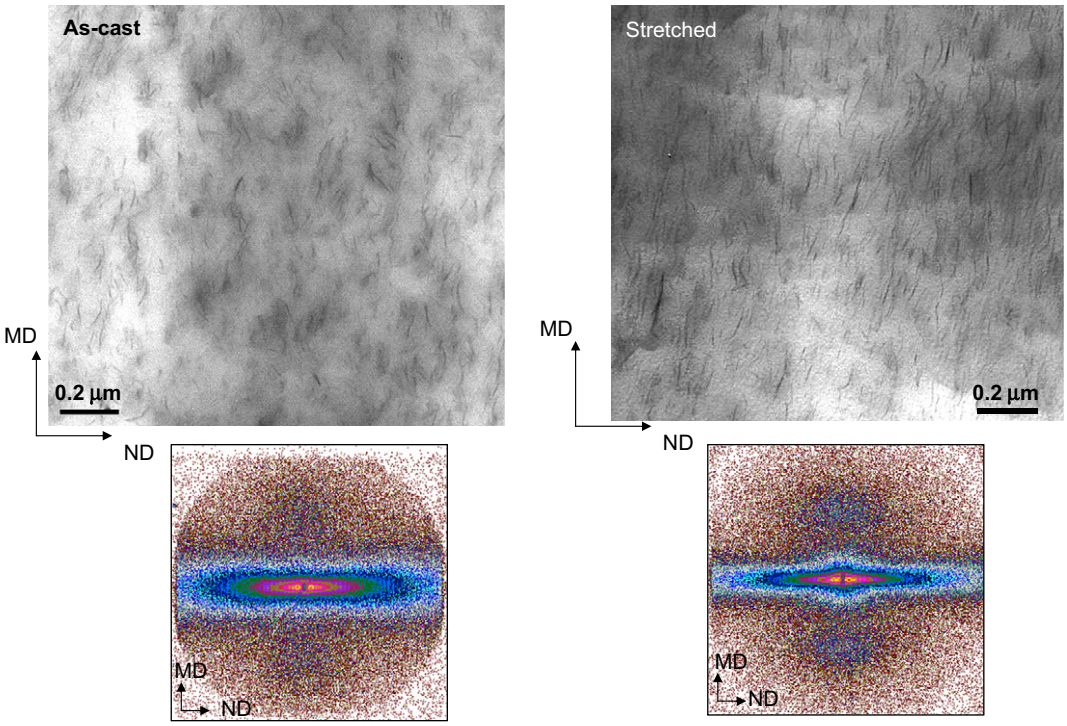

Fig. 16. TEM and corresponding SAXS images of as-cast and stretched (3×) nylon 6 nanocomposites at a loading of 3 wt%.

casting direction as evidenced from the highly aligned edges of the clay platelets in the stretched sample TEM image. One can also confirm the alignment of the clay edges by the reduction in the azimuthal spread of the streak pattern in the corresponding SAXS image indicating improved parallelism between the layers. Aligned edges on the MD–ND plane, however, is not enough to determine the 3D organization of the nanoplatelets. For this reason, we have also performed SAXS and TEM on the film plane (MD–TD) shown in Fig. 17. In the as-cast sample, the streak pattern does not exist. There is only a small ring around the beam stop as the X-ray beam being normal to the film surface is scattered by the clay platelets that are mostly in the plane of the film showing irregular correlations relative to each other. In the stretched sample,

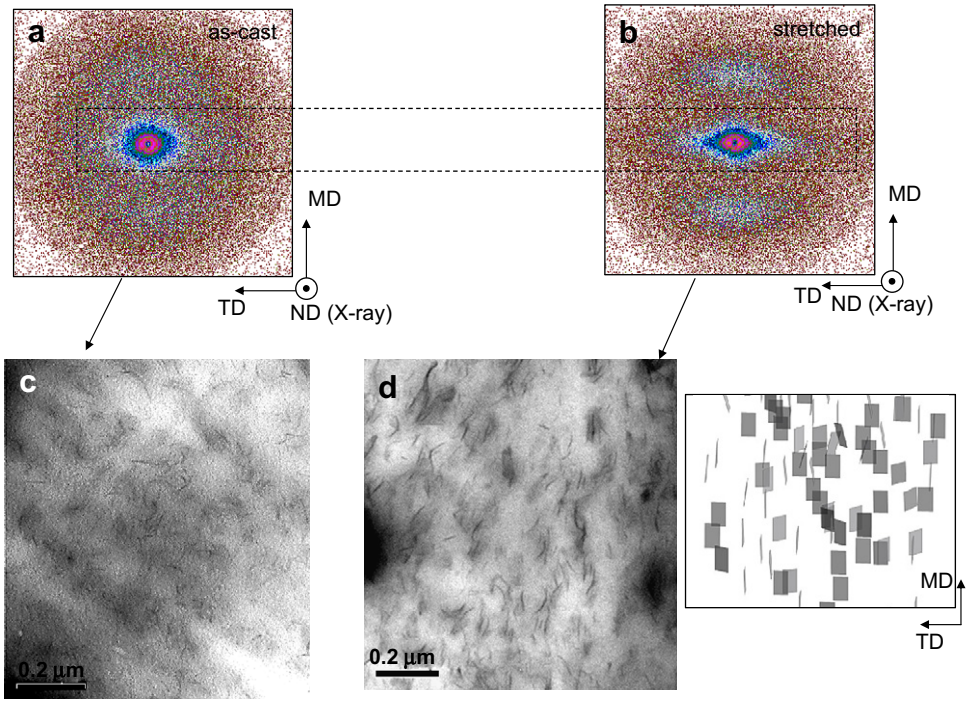

Fig. 17. SAXS images of (a) as-cast and (b) stretched (3×) nylon 6 nanocomposites at a loading of 3 wt%. (c) Model of aligned platelets and (d) TEM image of stretched sample on MD–TD and model.

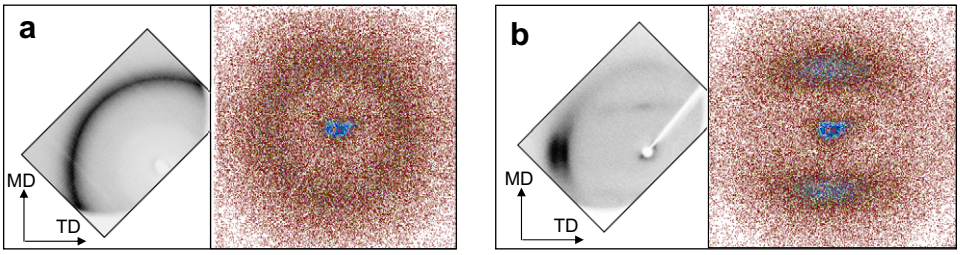

Fig. 18. WAXD and SAXS of (a) as-cast unfilled nylon 6 and (b) stretched unfilled nylon 6.

on the other hand, the streak pattern forms to some extent indicating that some of the clay edges start to appear on the film plane with some clay surfaces becoming normal to the film surface after stretching. The corresponding TEM image in Fig. 17d shows these clay edges in the stretched sample providing a further proof. However, the streak pattern and the orientation of these clay edges on the film plane (MD–TD) in the TEM image are not nearly as pronounced as that observed on the thickness plane (MD–ND).

These results indicate that stretching improves the parallelism between the nanolayers and orientation of the normals of the basal plane (001) of the nanoplatelets perpendicular to the machine direction. The majority of the platelets assumes increased planar orientation on the MD–TD with stretching. However, there are also those clay edges which had no orientation correlation on the film plane and form aligned edges normal to the film surface after stretching even on the film plane leading to a weak streak pattern on the MD–TD. This is indicating that uniaxial stretching of these films exhibiting initially planar texture begins to show structural signs to approach transverse isotropy.

Having established the state of clay orientation in the stretched samples, one can determine the effect of clay orientation on the measured in-plane film birefringence during stretching. Since unmodified montmorillonite nanoplatelets are negatively birefringent crystals ($n_{\text{out-of-plane}} = 1.485$, $n_{\text{in-plane}} = 1.505–1.550$) [54], their contribution to the measured in-plane birefringence should also be considered. In a previous publication we have shown that montmorillonite crystals dispersed in plasticized PVC lie mainly on their basal surfaces in the film plane upon compression molding [55] and do not contribute to the measured film birefringence [31]. Unmodified montmorillonite clay has zero in-plane birefringence since the refractive indices on the basal plane have the same value. However, the refractive index value normal to the basal plane (001) is smaller than the basal-plane (in-plane) refractive index values. Therefore, the clay nanoplatelets could contribute to measured film birefringence if they assume edge-on orientation parallel (positive contribution) or perpendicular (negative contribution) to the machine direction on the MD–TD plane. Based on our results, we expect birefringence contribution (increase) from the clay nanoplatelets to the measured film birefringence. However, the birefringence contribution is estimated to be low based on the clay loading and the small number of nanoplatelets that remain edge-on to the film surface only after stretching. One other reason would be the low intrinsic birefringence of clays (max $\Delta n_{\text{clay}} = -0.02$) [55] compared to that of the amorphous and crystalline phases of nylon 6,

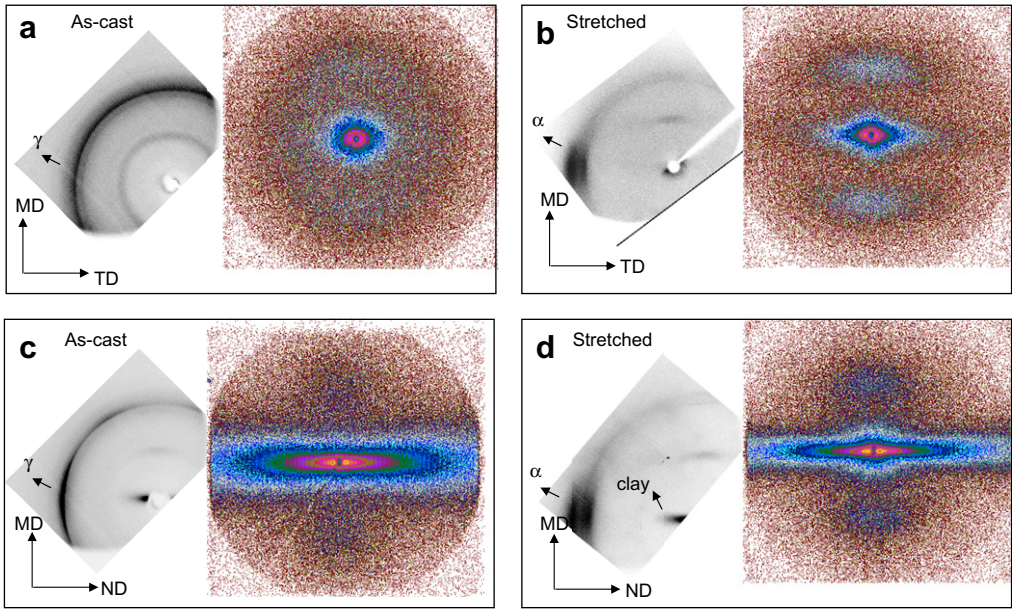

Fig. 19. SAXS of nylon 6 nanocomposites. (a) As-cast MD–TD, (b) stretched MD–TD, (c) as-cast MD–ND, and (d) stretched MD–ND.

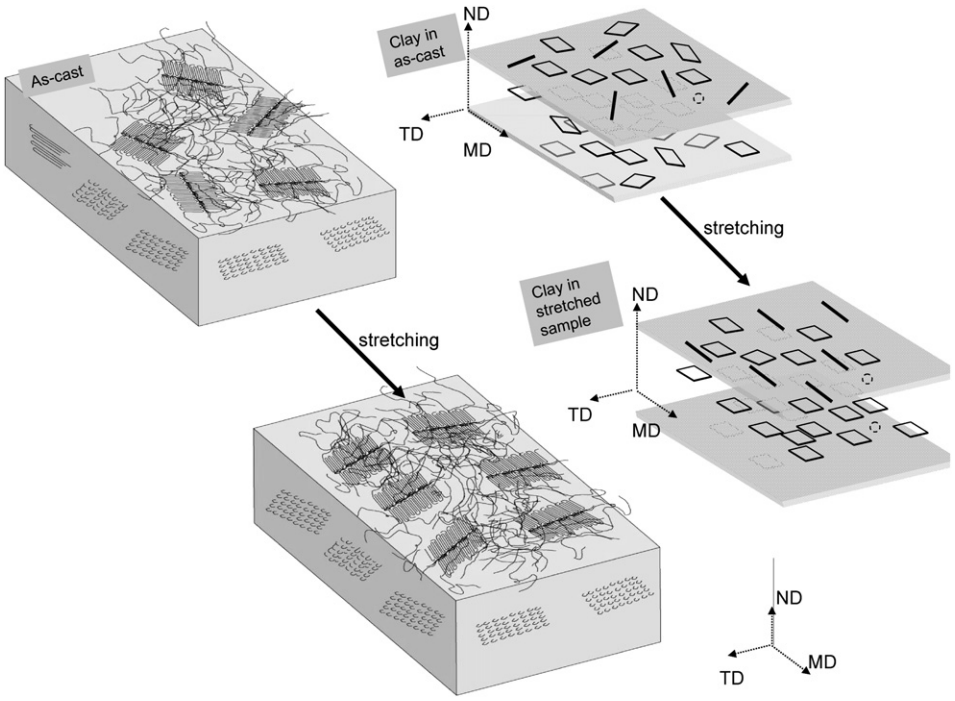

Fig. 20. Model for nylon 6 crystalline phase and clay orientation in as-cast and stretched nanocomposites.

especially alpha form observed in the stretched samples $\Delta n_{\text{crystal-alpha}} = 0.094$ [48], 0.089 [56]. $\Delta n_{\text{amorphous}} = 0.07858$. The in-plane and out-plane refractive indices of the montmorillonite particles would also change with the clay modification. Various birefringence values down to −0.003 were reported based on the complexes formed and their orientation with respect to the basal plane of the nanoplatelets [57].

Birefringence may arise not only from molecular anisotropy but also from an ordered arrangement of similar particles with larger sizes than molecules but smaller than the wavelength of light. This is known as form birefringence [58]. In order to determine whether the nanoplatelets are resulting in form birefringence, a simple analysis method given elsewhere [59] was applied to our system. In this analysis, an idealized case of a regular assembly of isotropic particles that have the form of thin plates was considered. We found that form birefringence due to the orderly arrangements of the nanoplatelets is a negligible quantity. This is because the thickness of the platelets is in the order of nanometers and the average refractive index of the nanoplatelets (∼1.512) [55] is close to the average refractive index of the surrounding medium nylon 6 (1.530) [57].

The influence of stretching on the crystal structure of the films was determined by the X-ray techniques (WAXD and SAXS) and ATR. In Section 3.1, we have determined that unfilled nylon 6 had a spherulitic structure. WAXD and SAXS patterns in Fig. 18 show that nylon 6 gets highly oriented with stretching. The SAXS pattern turns from an isotropic to a two point scattering pattern. The mechanism of structure formation in this case is simply deformation of nylon 6 spherulitic structure into highly oriented lamellar structure with cold drawing. We are not going to cover this area as this has been reported in detail in several past references [60–64]. In Fig. 19, WAXD and SAXS patterns are shown for as-cast and stretched nanocomposite samples. SAXS in Fig. 19 shows lamellae that have considerable in-plane isotropy on the MD–TD. Stretching results in the orientation of this lamellae leading to a two point pattern on the film plane. This is shown by a model in Fig. 20. The nanocomposite samples had already lamellar orientation in the MD–ND plane in their as-cast form as shown by the two point scattering pattern in Fig. 19c. With stretching, the two point pattern in the as-cast nanocomposite samples becomes even more pronounced. It is interesting to note that cold drawing at these temperatures does not destroy the lamellar structure.

4. Conclusions

The presence of nanoparticles (i) increases Young's modulus and (ii) delays strain-hardening behavior to large strains leading to increased toughness. Three important factors were determined to be influential for these improvements to occur. First, certain number of hydrogen bonding in the nanocomposite systems is eliminated. This loosens the strongly connected network that causes early strain hardening and ultimate failure in unfilled films. Second influential factor is the ability of the nanoplatelets to orient easily in a flow field due to their highly planar geometry. Third factor is the preferential crystallization and orientation of nylon 6 leading to small oriented crystallites on the film plane with increased slippage of easy shear planes. Evidences from these studies suggest that there is a critical loading level for these improvements to occur. Too much of the clay particles could lead to excessive disruption of the

hydrogen bonding network, overstiffness and high orientation of nylon 6 rendering the polymer unprocessable in typical film stretching processes resulting in premature fracture.

In these melt compounded nanocomposites, the modulus and toughness increase are simultaneously facilitated by the presence of nanoparticles as evidenced during stretching above the glass transition temperature. This is contrary to what is commonly reported for macrocomposites: in such macrocomposites, the increase in modulus by the addition of rigid particles nearly always comes at the expense of decrease in toughness.

References

[1] Kohan MI, editor. Nylon plastics. New York: Wiley; 1973.
[2] Nielsen LE. Mechanical properties of polymers and composites. New York: Marcel Dekker; 1974.
[3] Kojima M. J Mater Res 1993;8:1185–9.
[4] Usuki A, Koiwai A, Kojima Y, Kawasumi M, Okada A, Kuraichi T, et al. J Appl Polym Sci 1995;55:119–23.
[5] Yang F, Ou Y, Yu Z. J Appl Polym Sci 1998;69:355–61.
[6] Liu L, Qi Z, Zhu X. J Appl Polym Sci 1999;71:1133–8.
[7] Reynaud E, Jouen T, Gauthier C, Vigier G, Varlet J. Polymer 2001;42: 8759–68.
[8] Fornes TD, Yoon PJ, Keskkula H, Paul DR. Polymer 2001;42:9929–40.
[9] Cho JW, Paul DR. Polymer 2001;42:1083–94.
[10] Okada A, Usuki A. Mater Sci Eng 1995;C3:109–15.
[11] Vaia RA, Jandt KD, Kramer EJ, Giannelis EP. Chem Mater 1996;8: 2628–35.
[12] Giannelis EP. Appl Organomet Chem 1998;12:675–80.
[13] LeBaron PC, Wang Z, Pinnavaia TJ. Appl Clay Sci 1999;15:11–29.
[14] Ishida H, Campbell S, Blackwell J. Chem Mater 2000;12:1260–7.
[15] Alexandre M, Dubois P. Mater Sci Eng 2000;28:1–63.
[16] Yalcin B, Valladares D, Cakmak M. Polymer 2003;44(22):6913–25.
[17] Yalcin B, Cakmak M. Polymer 2004;45(8):2691–710.
[18] Giza E, Ito H, Kikutani T, Okui N. J Macromol Sci Phys Part B 2000;39: 545–59.
[19] Ergungor Z, Cakmak M, Batur C. Macromol Symp 2002;285:259–76.
[20] Subbotin A, Semenov AN, Manias E, Hadziioannou G, ten Brinke G. Macromolecules 1995;28:1511.
[21] Krishnamoorti R, Ren J, Silva AS. J Chem Phys 2002;114:4968–73.
[22] Koike Y, Cakmak M. Polymer 2003;44:4249–60.
[23] Kleppinger R, Van Es M. Polym Mater Sci Eng 2002;86:433–4.
[24] Varlot K, Reaynud E, Klopfer MH, Vigier G, Varlet J. J Polym Sci Part B Polym Phys 2001;39:1360–70.
[25] Reynaud E, Klopffer MH, Cavaille JY, Gauthier C, Varler J, Vigier G. Polym Mater Sci Eng 2000;82:219.
[26] Giza E, Ito H, Kikutani T, Okui N. J Polym Eng 2000;20:403–25.
[27] Fujiyama J, Cakmak M. 61st Annual technical conference – Society of Plastics Engineers, vol. 2; 2003. p. 1347–51.
[28] Mulligan J, Cakmak M. Macromolecules 2005;38(6):2333–44.
[29] Martins CI, Cakmak M. Macromolecules 2005;38(10):4260–73.
[30] Yalcin B, Cakmak M. J Polym Sci Phys 2005;43:724–42.
[31] Yalcin B, Arkin AH, Cakmak M, Hazer B, Erman B. Polymer 2006; 47(24):8183–93.
[32] Valladares D, Toki S, Sen TZ, Yalcin B, Cakmak M. Macromol Symp 2002;185:149–66.
[33] Sen TZ. Dissertation. Polymer Engineering Department, University of Akron; 2002.
[34] Beekmans F, Poshuma de Boer A. Macromolecules 1996;29: 8726–33.
[35] Kojima Y, Usuki A, Kawasumi M, Okada A, Kurauchi T, Kamigaito O, et al. J Polym Sci Part B 1994;32:625–30.
[36] Bafna A, Beaucage G, Mirabella F, Mehta S. Polymer 2003; 44(4):1103.
[37] Galgali G, Agarwal S, Lele A. Polymer 2004;45:6059–69.
[38] Malwitz MM, Lin-Gibson S, Hobbie EK, Butler PD, Gudrun S. J Polym Sci Part B 2003;41:3237–48.
[39] Holmes DR, Bunn CW, Smith DJ. J Polym Sci 1955;17:159.
[40] Arimoto H. J Polym Sci Part A 1964;2:2283.
[41] Arimoto H. Kobunshi Kagaku 1962;19:212.
[42] Miyasaka K, Makishima K. J Polym Sci Part A1 1967;5:3017.
[43] Miyasaka K, Ishikawa K. J Polym Sci Part A2 1968;6:1317.
[44] Ito M, Mizuochi K, Kanamoto T. Polymer 1998;39:4593–8.
[45] Lin L, Argon AS. Macromolecules 1992;25:4011–24.
[46] Penel-Pierron L, Séguéla R, Lefebvre J-M, Miri V, Depecker C, Jutigny M, et al. J Polym Sci Part B Polym Phys 2001;39:1224–36.
[47] Kunugi T, Yokokura S, Hashimoto M. J Chem Soc Jpn 1976;2:278.
[48] Murase S, Matsuda T, Hirami M. Macromol Mater Eng 2000;286(1): 48–51.
[49] Tonelli A, Kotek R. North Carolina State University National Textile Center annual report (project no: M01-S03); 2002.
[50] Roberts MF, Jenekhe SA. Macromolecules 1991;24:3142.
[51] Wu S. J Appl Polym Sci 1979;35:549.
[52] Wu S. Polymer 1985;26:1855.
[53] Muratoglu OK, Argon AS, Cohen RE, Weinberg M. Polymer 1995;36: 921–30.
[54] Greene KR. Clay Miner 1970;8:405.
[55] Yalcin B, Cakmak M. Polymer 2004;45(19):6623–38.
[56] Balcerzyk E, Kozlowski W, Wesolowska E, Lewaszkiewicz W. J Appl Polym Sci 1981;26(8):2573–80.
[57] Greene KR. Nature (London, UK) 1959;184(4):181.
[58] Wiener O. Abhandl Math Klas Kongl Sachs Gesellsch Wissensch 1912;23:509–604.
[59] Born M, Wolf E. Optics of crystals, Principles of optics. 6th ed. Pergamon Press; 1983. p. 705–08 [chapter XIV].
[60] Matsuo M, Hattori H, Nomura S, Kawai H. J Polym Sci Phys Ed 1976; 14:223–38.
[61] Galeski A, Argon AS, Cohen RE. Macromolecules 1988;21:2761–70.
[62] Zhou H, Wilkes GL. J Mater Sci 1998;33:287–303.
[63] Samuels RJ. J Polym Sci Part C 1967;20:253–84.
[64] Nozue Y, Shinohara Y, Ogawa Y, Sakurai T, Hori H, Kasahara T, et al. Macromolecules 2007;40:2036–45.